Photon-induced suppression of interlayer tunneling in van der Waals heterostructures

Woo-Ram Lee and Wang-Kong Tse

Phys. Rev. B **99**, 201403 — Published 6 May 2019

DOI: 10.1103/PhysRevB.99.201403

Photon-Induced Suppression of Interlayer Tunneling in Van Der Waals Heterostructures

Woo-Ram Lee and Wang-Kong Tse
Department of Physics and Astronomy, The University of Alabama, Alabama 35487, USA
Center for Materials for Information Technology,
The University of Alabama, Alabama 35401, USA

We develop a theory for interlayer tunneling in van der Waals heterostructures driven under a strong electromagnetic field, using graphene/h-BN/graphene as a paradigmatic example. Our theory predicts that strong anti-resonances appear at bias voltage values equal to an integer multiple of the light frequency. These features are found to originate from photon-assisted resonant tunneling transitions between Floquet sidebands of different graphene layers, and are unique to two-band systems due to the interplay of both intraband and interband tunneling transitions. Our results point to the possibility of tunneling localization in van der Waals heterostructures using strong electromagnetic fields.

When light is incident on a tunneling junction, inelastic tunneling transitions can occur via the exchange of photons between electrons and the electromagnetic field. This photon-assisted tunneling (PAT) phenomenon was first predicted in the classic work by Tien and Gordon [1] in superconductor-insulator-superconductor tunneling junctions [2]. PAT has since been studied and observed in many systems [3], including semiconductor quantum dots [4–6], double quantum wells [7, 8] and superlattices [9, 10], and optical lattices [11, 12]. In particular, tunneling dynamics can be suppressed [13–15] when the light coupling parameter, given by the ratio of the driving field amplitude and frequency, matches a zero of the Bessel function, a celebrated phenomenon called dynamic localization [16].

Van der Waals heterostructures (vdWHs) [17] are an emerging class of nanoscale materials that hold great promise as a platform for realizing unconventional electronic properties and desirable functionalities. Vertically stacked vdWHs exhibit many distinctive properties not available in conventional semiconductor quantum well systems, including enhanced longitudinal and Hall Coulomb drag [18], tunable metal-insulator transition [19] and extraordinary photovoltaic response [20]. In addition to in-plane transport, vertical tunneling transport in a field-effect tunneling junction geometry exhibits superior current-voltage characteristics [21–25].

A strong electromagnetic field can provide a heretofore unexplored degree of freedom for tuning the tunneling dynamics in vdWHs. In this work, we theoretically investigate interlayer tunneling in optically driven vertical vdWHs, using graphene/h-BN/graphene as an archetypical system. Using the Keldysh-Floquet Green's function formalism, we formulate a theory for the non-equilibrium PAT current and elucidate the non-perturbative effects of the driving field on the intraband and interband tunneling transitions. Our theory predicts a new type of tunneling localization effect where photon-enabled resonant tunneling processes induce a dramatic suppression of the interlayer tunneling current as a function of the bias voltage, precisely at integer multiples of the photon energy.

Model — Our tunneling structure consists of two parallel graphene layers, labeled as top (T) and bottom (B), that are separated by a middle insulating monolayer of hexagonal boron nitride (h-BN). The layers are perfectly aligned and stacked in the ABA (Bernal) configuration, and a bias voltage V is applied across the top and bottom layers. The low-energy excitations around the K and K' points (labeled by $\xi = \pm 1$, respectively) in the Brillouin zone of each graphene layer is governed by the 2D massive Dirac model up to an energy cutoff $\mathcal{E}_c \approx 2.68\,\text{eV}$:

$$h_{\mathbf{k}\xi T,B} = v\hbar(\xi k_x\sigma_x + k_y\sigma_y) + \Delta\sigma_z/2 \pm eV\mathbb{I}_2/2, \quad (1)$$

where $v \approx 10^6\,\text{m/s}$ is the Dirac velocity, $\Delta \approx 20\,\text{meV}$ is the band gap induced by the h-BN layer [26], $-e$ is the electron charge, and $\{\mathbb{I}_2, \sigma_x, \sigma_y, \sigma_z\}$ denote the identity and Pauli matrices in the sublattice-pseudospin (*i.e.*, a and b sites) space. We construct the Hamiltonian of the trilayer system in a nearest-neighbor hopping approximation, including the coupling between each graphene layer and the h-BN layer and ignoring the negligible direct hopping between the graphene sheets. Due to the large band gap $\Delta_{\text{BN}} \approx 4.82\,\text{eV}$ [27], we can trace out the h-BN layer and obtain an effective double-layer Hamiltonian [28] $\tilde{\mathcal{H}} = \sum_{\mathbf{k}}\sum_{\xi=\pm1}\tilde{\psi}^\dagger_{\mathbf{k}\xi}(\tilde{h}_{\mathbf{k}\xi}+\tilde{\mathcal{W}})\tilde{\psi}_{\mathbf{k}\xi}$, where $\tilde{\psi}^\dagger_{\mathbf{k}\xi} = (\phi^\dagger_{\mathbf{k}\xi T}, \phi^\dagger_{\mathbf{k}\xi B})$. Tilde symbolizes the layer-pseudospin (*i.e.*, T and B) space. It is convenient to define $\mathbb{I}_\pm = (\mathbb{I}_2 \pm \sigma_z)/2$, $\tilde{\mathbb{I}}_\pm = (\tilde{\mathbb{I}}_2 \pm \tilde{\sigma}_z)/2$, $\tilde{\sigma}_\pm = (\tilde{\sigma}_x \pm i\tilde{\sigma}_y)/2$ and use the new basis $\{\tilde{\mathbb{I}}_+, \tilde{\mathbb{I}}_-, \tilde{\sigma}_+, \tilde{\sigma}_-\}$ for the layer pseudospins to write the unperturbed Hamiltonian as $\tilde{h}_{\mathbf{k}\xi} = h_{\mathbf{k}\xi T}\otimes\tilde{\mathbb{I}}_+ + h_{\mathbf{k}\xi B}\otimes\tilde{\mathbb{I}}_-$ and the interlayer tunneling Hamiltonian as $\tilde{\mathcal{W}} = \mathcal{W}_{TB}\otimes\tilde{\sigma}_+ + \mathcal{W}_{BT}\otimes\tilde{\sigma}_-$. The tunneling matrix elements are given by $\mathcal{W}_{TB} = \mathcal{W}^\dagger_{BT} = \mathcal{W}_0\mathbb{I}_-$ with $\mathcal{W}_0 = -2\Gamma^2_{ab}\Delta^{-1}_{\text{BN}}$, where $\Gamma_{ab} \approx 0.4\,\text{eV}$ is the interlayer hopping energy from a site in graphene to b site in h-BN (or vice versa) [27].

We consider the two graphene layers to be coupled, for simplicity, to the same optical field by imagining two

independent but identical laser sources setup symmetrically on both sides of the vdWH, illuminating the two graphene layers at normal incidence. Thus, the surface electric fields on both layers will be in phase with the same amplitude and frequency. Choosing the propagation direction along the z axis, the incident light with electric field amplitude E, frequency Ω, and polarization ϑ is described by the vector potential $\mathbf{A}(t) = (cE/\Omega)[\sin(\Omega t)\hat{x} + \sin(\Omega t + \vartheta)\hat{y}]$. The Peierls substitution $\hbar\mathbf{k} \to \hbar\mathbf{k} + e\mathbf{A}(t)/c$ in the original Hamiltonian produces the time-dependent Hamiltonian $\tilde{\mathcal{H}}_{\mathbf{k}\xi}(t) = \tilde{\mathcal{H}}_{\mathbf{k}\xi} + \tilde{\mathcal{V}}_\xi(t)$, with the interaction $\tilde{\mathcal{V}}_\xi(t) = \mathcal{V}_\xi(t) \otimes \tilde{\mathbb{I}}_2$, where $\mathcal{V}_\xi(t) = \mathcal{V}_0[\xi \sin(\Omega t)\sigma_x + \sin(\Omega t + \vartheta)\sigma_y]$. The ratio $\mathcal{V}_0/\Delta = (E/E_0)/(\hbar\Omega/\Delta)$ with $E_0 = \Delta^2/(ev\hbar)$ describes the interaction amplitude in dimensionless form.

Theory — Our formalism is developed by treating the interlayer tunneling Hamiltonian as a perturbation while taking into account the optical field non-perturbatively. Noting that the total charge is conserved in the system, the interlayer electric current density takes the form [29] $J(t) = 2S^{-1}\langle \hat{I}(t)\rangle$, where 2 counts the spin degeneracy, S is the normalization area, $\langle\cdots\rangle$ is the canonical ensemble average, and $\hat{I}(t) = \partial_t \hat{Q}_T(t) = -\partial_t \hat{Q}_B(t) = (i/\hbar)[\tilde{\mathcal{H}}(t), \hat{Q}_T(t)]$ is the electric current with $\hat{Q}_{T,B}(t)$ being the electric charge operator on layer T and B. The time evolution of $J(t)$ is determined from the equal-time lesser Green's function, $G^<_{\mathbf{k}\xi}(t,t)$. In a non-equilibrium steady state (NESS), the system respects time translational symmetry and is thus governed by the Floquet theorem [31]. By using the Floquet mode expansion of the Green's function [32], we obtain the time-averaged interlayer electric current density $J = -4(e/\hbar)(1/S)\sum_{\mathbf{k}}\sum_{\xi=\pm1}\int_{-\hbar\Omega/2}^{\hbar\Omega/2}(d\hbar\omega/2\pi)\,\mathrm{Re}\mathrm{Tr}\big\{[\mathcal{W}_{BT}\otimes\hat{\mathbb{I}}_\infty][\hat{G}^<_{\mathbf{k}\xi}(\omega)]_{TB}\big\}$, where an overhat refers to a quantity in the Floquet space, the subscript "TB" of the Green's function refers to its off-diagonal element in the layer subspace, "Tr" is the trace over sublattice pseudospins and Floquet modes, and $\hat{\mathbb{I}}_n$ is the $n\times n$ identity matrix in the Floquet space.

The lesser Green's function $\hat{G}^<_{\mathbf{k}\xi}$ can be calculated within the Keldysh-Floquet Green's function formalism [35–37]. The full, tunneling-coupled Green's function is uniquely determined by the uncoupled Green's function of each layer and the interlayer tunneling Hamiltonian via the Dyson equation in the Keldysh-Floquet space [38]. Expansion of $\hat{G}^<_{\mathbf{k}\xi}$ up to first order in $\mathcal{W}_0$ yields the following *photon-assisted* tunneling current formula:

$$J_{\mathrm{tun}} = -4\frac{e}{\hbar}\frac{1}{S}\sum_{\mathbf{k}}\sum_{\xi=\pm1}\int_{-\hbar\Omega/2}^{\hbar\Omega/2}\frac{d\hbar\omega}{2\pi} \times \mathrm{Re}\Big\{\mathrm{Tr}\big[\hat{\mathbb{W}}^\dagger_{\mathbf{k}\xi TB}(\omega)\hat{\mathcal{G}}^R_{\mathbf{k}\xi T}(\omega)\hat{\mathbb{W}}_{\mathbf{k}\xi TB}(\omega)\hat{g}^<_{\mathbf{k}\xi B}(\omega) + \hat{\mathbb{W}}^\dagger_{\mathbf{k}\xi BT}(\omega)\hat{\mathcal{G}}^A_{\mathbf{k}\xi B}(\omega)\hat{\mathbb{W}}_{\mathbf{k}\xi BT}(\omega)\hat{g}^<_{\mathbf{k}\xi T}(\omega)\big]\Big\}. \quad (2)$$

This result is central to this paper. Its formal structure is familiar from the conventional tunneling theory [34], except that all the Green's functions and tunneling amplitudes are now dependent on the electromagnetic field. $\hat{\mathcal{G}}^R_{\mathbf{k}\xi T,B}(\omega)$ is the retarded Floquet Green's function of the T and B layers, and $\hat{g}^<_{\mathbf{k}\xi T,B}(\omega)$ is the lesser Floquet Green's function in the absence of light. Coupling to metallic leads provides an energy relaxation mechanism under the adiabatic switch-on of the optical field [38], and enters into the Green's functions as the broadening parameter Γ. The tunneling process is renormalized by light and is described by an effective *photon-dressed* interlayer tunneling Hamiltonian

$$\hat{\mathbb{W}}_{\mathbf{k}\xi\alpha\bar{\alpha}}(\omega) = \mathcal{W}_{\alpha\bar{\alpha}}\big[\mathbb{I}_2\otimes\hat{\mathbb{I}}_\infty + \hat{\mathcal{G}}^R_{\mathbf{k}\xi\bar{\alpha}}(\omega)\hat{\mathcal{V}}_\xi\big], \quad (3)$$

where $\alpha \in \{T, B\}$ and the overbar denotes a complement, *e.g.*, $\bar{T} = B$. It shows that non-perturbative photon dressing effects affect not only the electronic spectrum (through the Floquet Green's functions), but also the tunneling amplitude through the second term within the brackets in Eq. (3).

To illustrate the physics contained in Eq. (2) and also to connect with the more familiar case without light, let us first consider the weak coupling regime [35, 51] defined as $\mathcal{V}_0/\hbar\Omega \ll 1$. In this scenario the photon-induced correction $\sim \hat{\mathcal{G}}^R\hat{\mathcal{V}}$ to the tunneling Hamiltonian [Eq. (3)] is negligible and the electronic distribution function of the graphene layers retain a quasi-equilibrium form. For the ABA stacking configuration of our system, $[\mathcal{W}_{TB}]_{cc'} = [\mathcal{W}_{BT}]^*_{c'c} = \mathcal{W}_0\delta_{cc'}\delta_{cb}$ where $c, c' \in \{a, b\}$ label the sublattice pseudospins, we can reduce Eq. (2) to a compact form

$$\frac{J_{\mathrm{tun}}}{J_0} = \frac{(2\pi v\hbar)^2}{\Delta}\frac{1}{S}\sum_{\mathbf{k}}\sum_{\xi=\pm1}\int_{-\infty}^{\infty}d\hbar\tilde{\omega} \times\big[\rho^{(\mathrm{ph})}_{\mathbf{k}\xi Bb}(\tilde{\omega})\rho^{(\mathrm{eq})}_{\mathbf{k}Tb}(\tilde{\omega})f_T(\tilde{\omega}) - \rho^{(\mathrm{ph})}_{\mathbf{k}\xi Tb}(\tilde{\omega})\rho^{(\mathrm{eq})}_{\mathbf{k}Bb}(\tilde{\omega})f_B(\tilde{\omega})\big], \quad (4)$$

where $J_0 = e\Delta|\mathcal{W}_0|^2/(\pi v^2\hbar^3)$ is a characteristic tunneling current density, and $\tilde{\omega} \equiv \omega + n\Omega$ is the frequency in the extended zone scheme [32]. The two terms of Eq. (4) correspond to a forward and a backward tunneling channel, and each channel is modified by non-perturbative light coupling effects through the Floquet mode spectral function $\rho^{(\mathrm{ph})}_{\mathbf{k}\xi\alpha b}(\tilde{\omega}) = -\pi^{-1}\mathrm{Im}[\hat{\mathcal{G}}^R_{\mathbf{k}\xi\alpha}(\omega)]_{bb;nn}$. In the absence of optical fields, $\rho^{(\mathrm{ph})}_{\mathbf{k}\xi\alpha b}(\tilde{\omega})$ recovers its equilibrium counterpart $\rho^{(\mathrm{eq})}_{\mathbf{k}\alpha b}(\tilde{\omega}) = -\pi^{-1}\mathrm{Im}[\hat{g}^R_{\mathbf{k}\xi\alpha}(\omega)]_{bb;nn}$ with Eq. (4) reducing to the well-known 2D-to-2D tunneling current formula [52, 53]. Fig. 1(a) shows the Floquet mode spectral function $\rho^{(\mathrm{ph})}_{\mathbf{k}\xi\alpha b}(\tilde{\omega})$ as a function of the equilibrium energy dispersion $\mathcal{E}_{\mathbf{k}}$ for different values of the driving field E. At small values of E, the quasienergy dispersions of the Floquet sidebands (*i.e.*, photon-dressed electronic bands) approximately coincide with copies of the equilibrium bands shifted by

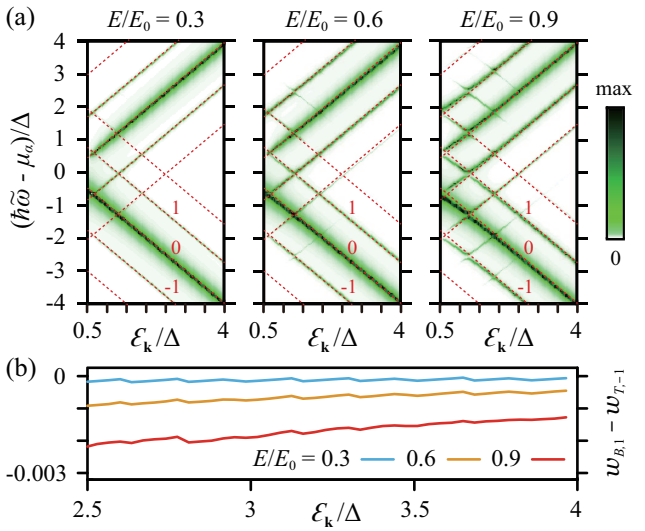

FIG. 1: (a) Floquet mode spectral function $\rho^{(\mathrm{ph})}_{\mathbf{k}\xi\alpha b}(\tilde{\omega})$ for valley K', layer $\alpha \in \{T, B\}$, and sublattice b as a function of $\mathcal{E}_{\mathbf{k}}$ for different values of E/E_0. The red dotted lines are guidelines denoting the equilibrium bands and their corresponding copies shifted by integer multiples of $\hbar\Omega$. Three main Floquet sidebands belonging to $\gamma = -1$ are indexed by red-colored integers. Parameters used are $\Gamma/\Delta = 0.01$, $\varphi_{\mathbf{k}} = 0$, $\hbar\Omega/\Delta = 1.25$, and $\vartheta = \pi/2$. (b) Difference between the spectral weights $w_{B,n=1} - w_{T,n=-1}$ of the Floquet valence sidebands $n = \pm 1$ as a function of $\mathcal{E}_{\mathbf{k}}$ for different values of E/E_0. For the parameters of graphene in Eq. (1), $E_0 \approx 608\,\mathrm{kV/m}$.

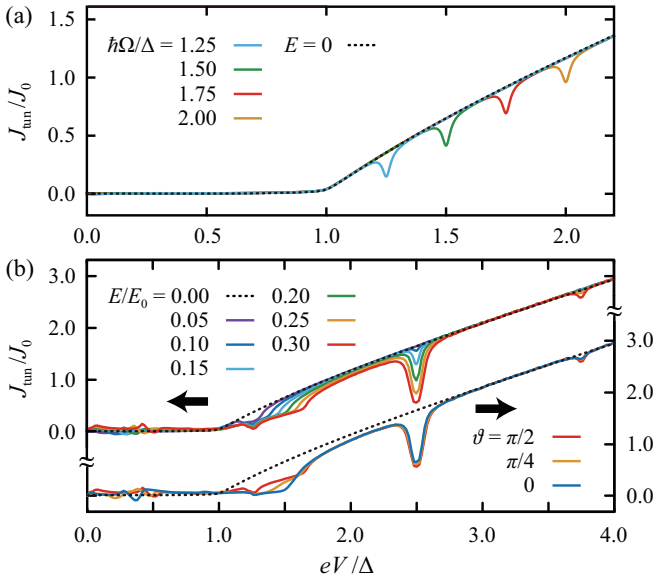

FIG. 2: Photon-assisted tunneling current density J_{tun} in units of J_0 as a function of bias voltage V. (a) Solid lines show the numerical results obtained from the second-order perturbation theory for a fixed $E/E_0 = 0.015$ and different values of Ω. The dashed line shows the dark tunneling current. (b) Exact numerical results [Eqs. (2)-(3)] for $\hbar\Omega/\Delta = 1.25$. The upper set of solid lines shows the tunneling current at a fixed polarization angle $\vartheta = \pi/2$ for different values of the optical field strength E. The lower set of solid lines shows the tunneling current at a fixed $E/E_0 = 0.3$ for different values of polarization angle ϑ. In all figures, we use the common parameters $k_BT/\Delta = 0.02$, $\Gamma/\Delta = 0.01$, and $\mathcal{E}_c/\Delta = 4$ [59]. The scale of the tunneling current density is $J_0 \approx 15.8\,\mathrm{mA}/\mu\mathrm{m}^2$.

integer multiples of $\hbar\Omega$, and the reduced-zone Floquet quasienergy $\bar{\mathcal{E}}_{\mathbf{k}} \approx \mathcal{E}_{\mathbf{k}}$. The undressed conduction and valence bands each generate their own Floquet sidebands, which for convenience will be called Floquet conduction and valence sidebands (FCSB and FVSB, respectively). As E increases, mixing between Floquet states becomes stronger and quasienergy band gaps appear prominently at the locations of anti-crossing, given by $(\mathcal{E}_{\mathbf{k}}, \hbar\tilde{\omega} - \mu_\alpha) = (m - n, m + n)\hbar\Omega/2$ with $m, n \in \mathbb{Z}$.

Single-photon excitations — Before carrying out fully numerical calculations of Eq. (2), we first perform a second-order perturbative analysis in the driving field amplitude. In this work, we focus on low temperatures $k_BT \ll \Delta$ and evaluate the tunneling current, assuming each graphene layer is at half-filling so that the electrochemical potential under bias is $\mu_T = -\mu_B = eV/2$ [54]. Treating the optical field $\mathcal{V}_\xi(t)$ as a perturbation and expanding the single-layer Green's function into $\hat{\mathcal{G}}_{\mathbf{k}\xi\alpha}(\omega) = \sum_{j=0,1,2}(\mathcal{V}_0)^j \hat{\mathcal{G}}^{(j)}_{\mathbf{k}\xi\alpha}(\omega) + \mathcal{O}(\mathcal{V}_0^3)$ [28], Eq. (2) can be written in the form $J_{\mathrm{tun}} = \sum_{j=0,1,2}(\mathcal{V}_0)^j J^{(j)}_{\mathrm{tun}} + \mathcal{O}(\mathcal{V}_0^3)$, where the zeroth-order term [55] yields the dark tunneling current [56–58]. Fig. 2(a) shows, for different values of frequency, the tunneling current $J_{\mathrm{tun}} = J^{(0)}_{\mathrm{tun}} + \mathcal{V}_0^2 J^{(2)}_{\mathrm{tun}}$ obtained within the present second-order perturbation theory. It is seen that the overall profile remains close to the dark tunneling current $J^{(0)}_{\mathrm{tun}}$ (dashed line) except at $eV = \hbar\Omega$. When the bias voltage is equal to the photon energy, single-photon assisted tunneling transitions occur, manifesting as a single anti-resonance in the second-order contribution $J^{(2)}_{\mathrm{tun}}$.

Photon-assisted tunneling suppression — To account for strong field and multiphoton excitation effects, we now evaluate the tunneling current from Eqs. (2)-(3) non-perturbatively. Fig. 2(b) shows our full numerical results for different field strengths E (upper set of solid lines) and for different polarization angles ϑ (lower set) with an optical frequency value $\hbar\Omega = 1.25\Delta$ slightly larger than the band gap. For this frequency value and up to the maximum field strength $E/E_0 = 0.3$, $\mathcal{V}_0/\hbar\Omega < 1$ always. In the absence of light, the dark tunneling current remains zero when the bias voltage is smaller than the band gap, as shown by the dashed lines in both Figs. 2(a)-(b). When light is turned on, we first notice that the PAT current becomes non-zero even when $eV < \Delta$, a feature not captured by the second-order perturbation theory. For bias values greater than the band gap $eV > \Delta$, our theory predicts periodic anti-resonance suppression of the tunneling current with a separation $\hbar\Omega$ along the bias

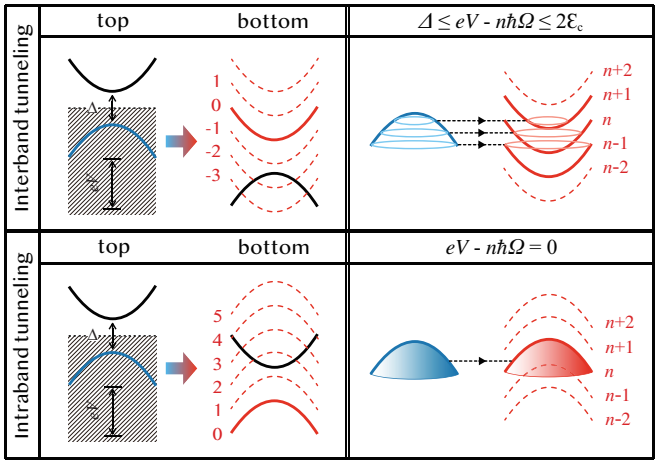

FIG. 3: Schematic for forward tunneling transitions for $eV > 0$. The left panel depicts the interband and intraband tunneling mechanisms assisted by multiphoton processes. The Floquet sidebands are indexed by red-colored integers. The right panel depicts the resonance tunneling conditions for the interband (or intraband) tunneling processes from the undressed valence band of the top layer to a Floquet conduction (or valence) sideband of the bottom layer. Backward tunneling transitions can be visualized similarly from Eq. (4).

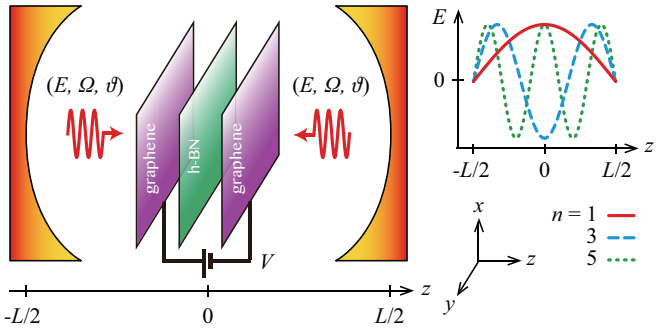

FIG. 4: Schematic for experimental proposal. Graphene/*h*-BN/Graphene heterostructure is positioned at the center of the optical cavity (left), in which an odd cavity mode is established (right).

voltage axis as seen in Fig. 2(b). Remarkably, the anti-resonance positions are found to be independent of the field strength E and polarization angle ϑ, and are precisely given by integer multiples of $\hbar\Omega$, *i.e.*, $eV = N\hbar\Omega$ with $N \in \mathbb{Z}$. Close to the band gap $eV \gtrsim \Delta$ in particular, we find a dramatic suppression of the PAT current to almost zero from its dark value due to the first anti-resonance located at $eV = \hbar\Omega = 1.25\Delta$. Fig. 2(b) also shows that the strength of the anti-resonances increases with the field strength, resulting in a progressive suppression of the tunneling current [60] and indicating a tendency towards complete localization at stronger fields. Note here that the nature of our predicted tunneling suppression under optical illumination is fundamentally different from dynamic localization [16, 31, 61], which occurs only when the coupling parameter $\mathcal{V}_0/\hbar\Omega$ is equal to a zero of the Bessel function.

The periodic occurrence of the tunneling suppression uncovered by our calculations stems from resonant intraband tunneling assisted by multiphoton excitations. Let us first consider the case without illumination. Due to conservation of in-plane momentum, conventional 2D-to-2D resonant tunneling in coupled semiconductor quantum wells occurs when the layers' band dispersions are closely aligned whereby $J_{\rm tun} \sim \tau$ becomes sharply peaked (here τ is the electron's lifetime) [62]. Graphene allows for interband tunneling when the bias voltage exceeds the band gap. If illumination is absent in our system, only interband (but not intraband) tunneling can occur since the layers' Fermi levels are assumed to be inside the band gap. However, an optical driving field opens up many additional channels for intraband tunneling via photon-assisted transitions between Floquet sidebands (see Fig. 3). When one layer's undressed valence band (VB) edge is aligned with one of the many FVSB edges of the other layer, electron momentum and energy conservation are simultaneously satisfied and resonant tunneling can occur. This Floquet band edge alignment happens when the bias voltage is tuned to an integer multiple of the driving frequency. To understand why a suppression instead of an enhancement occurs, it is useful to refer to Eq. (4) under a forward bias condition $eV > 0$. Physically, the forward tunneling contribution involves tunneling from the undressed VB in the *top* layer to the $n > 0$ FVSBs in the *bottom* layer (Fig. 3), while the backward tunneling contribution involves tunneling from the undressed VB in the *bottom* layer to the $n < 0$ FVSBs in the *top* layer. Because they are further removed from the $n < 0$ FCSBs, the $n < 0$ FVSBs carry a higher spectral weight than their $n > 0$ counterparts [63], as confirmed by our numerical calculations of integrated spectral weights of the Floquet mode spectral function [Fig. 1(b)]. As a result, under the resonant condition $eV = N\hbar\Omega$, the backward tunneling contribution is dramatically enhanced causing a suppression of $J_{\rm tun}$ [64].

Proposed experimental setup — We close by commenting on observability in experiments. To realize the condition with the same electric field amplitudes on both layers, two scenarios can be devised. First, this condition can be approximately achieved when the laser wavelength is long compared with the thickness of the vdWH [65]. Second, an optical cavity can be used (see Fig. 4). When the cavity mode of the standing wave is odd and the vdWH is placed at the cavity's center, both graphene layers will experience the same electromagnetic field.

The resonant intraband tunneling mechanism we discovered is a generalization of the usual dark resonant tunneling to the scenario with Floquet sidebands under strong optical illumination. This phenomenon should apply not only to graphene layers, but also to trilayer vd-

WHs with other 2D materials such as bilayer graphene and transition-metal dichalcogenides. The fact that the tunneling current can be turned on and off by illumination at frequency values equal to an integral fraction of the bias voltage suggests a time-dependent control scheme for switching applications, opening the door to dynamical tuning of tunneling dynamics using periodic drives.

We thank Patrick Kung, Takashi Oka, and Godfrey Gumbs for useful discussions. This work was supported by startup funds from the University of Alabama and the U.S. Department of Energy, Office of Science, Basic Energy Sciences under Early Career Award #DE-SC0019326.

[1] P. K. Tien and J. P. Gordon, Multiphoton Process Observed in the Interaction of Microwave Fields with the Tunneling between Superconductor Films, Phys. Rev. **129**, 647 (1963).

[2] A. H. Dayem and R. J. Martin, Quantum Interaction of Microwave Radiation with Tunneling Between Superconductors, Phys. Rev. Lett. **8**, 246 (1962).

[3] G. Platero and R. Aguado, Photon-assisted transport in semiconductor nanostructures, Phys. Rep. **395**, 1 (2004).

[4] L. P. Kouwenhoven, S. Jauhar, K. McCormick, D. Dixon, P. L. McEuen, Yu. V. Nazarov, N. C. van der Vaart, and C. T. Foxon, Photon-assisted tunneling through a quantum dot, Phys. Rev. B **50**, 2019(R) (1994).

[5] L. P. Kouwenhoven, S. Jauhar, J. Orenstein, P. L. McEuen, Y. Nagamune, J. Motohisa, and H. Sakaki, Observation of Photon-Assisted Tunneling through a Quantum Dot, Phys. Rev. Lett. **73**, 3443 (1994).

[6] C. A. Stafford and N. S. Wingreen, Resonant Photon-Assisted Tunneling through a Double Quantum Dot: An Electron Pump from Spatial Rabi Oscillations, Phys. Rev. Lett. **76**, 1916 (1996).

[7] H. Drexler, J. S. Scott, S. J. Allen, K. L. Campman, and A. C. Gossard, Photon-assisted tunneling in a resonant tunneling diode: Stimulated emission and absorption in the THz range, Appl. Phys. Lett. **67**, 2816 (1995).

[8] F. T. Vasko and E. P. OReilly, Resonant photon-assisted tunneling between independently contacted quantum wells, Phys. Rev. B **67**, 235317 (2003).

[9] B. J. Keay, S. J. Allen Jr., J. Galán, J. P. Kaminski, K. L. Campman, A. C. Gossard, U. Bhattacharya, and M. J. W. Rodwell, Photon-Assisted Electric Field Domains and Multiphoton-Assisted Tunneling in Semiconductor Superlattices, Phys. Rev. Lett. **75**, 4098 (1995).

[10] G. S. Vieira, S. J. Allen, P. S. S. Guimarães, K. L. Campman, and A. C. Gossard, Resonantly enhanced photon-assisted tunneling in a multiple-quantum-well superlattice, Phys. Rev. B **58**, 7136 (1998).

[11] C. Sias, H. Lignier, Y. P. Singh, A. Zenesini, D. Ciampini, O. Morsch, and E. Arimondo, Observation of Photon-Assisted Tunneling in Optical Lattices, Phys. Rev. Lett. **100**, 040404 (2008).

[12] R. Ma, M. E. Tai, P. M. Preiss, W. S. Bakr, J. Simon, and M. Greiner, Photon-Assisted Tunneling in a Biased Strongly Correlated Bose Gas, Phys. Rev. Lett. **107**, 095301 (2011).

[13] B. J. Keay, S. Zeuner, S. J. Allen Jr, K. D. Maranowski, A. C. Gossard, U. Bhattacharya, and M. J. W. Rodwell, Dynamic localization, absolute negative conductance, and stimulated, multiphoton emission in sequential resonant tunneling semiconductor superlattices, Phys. Rev. Lett. **75**, 4102 (1995).

[14] K. W. Madison, M. C. Fischer, R. B. Diener, Qian Niu, and Mark G. Raizen, Dynamical Bloch band suppression in an optical lattice, Phys. Rev. Lett. **81**, 5093 (1998).

[15] S. Longhi, M. Marangoni, M. Lobino, R. Ramponi, P. Laporta, E. Cianci, and V. Foglietti, Observation of dynamic localization in periodically curved waveguide arrays, Phys. Rev. Lett. **96**, 243901 (2006).

[16] D. H. Dunlap, and V. M. Kenkre, Dynamic localization of a charged particle moving under the influence of an electric field, Phys. Rev. B **34** 6, 3625 (1986).

[17] I. V. Antonova, Vertical Heterostructures Based on Graphene and Other 2D Materials, Semiconductors **50**, 66 (2016).

[18] R. V. Gorbachev, A. K. Geim, M. I. Katsnelson, K. S. Novoselov, T. Tudorovskiy, I. V. Grigorieva, A. H. MacDonald et al., Strong Coulomb drag and broken symmetry in double-layer graphene, Nature Phys. **8**, 896 (2012).

[19] L. A. Ponomarenko, A. K. Geim, A. A. Zhukov, R. Jalil, S. V. Morozov, K. S. Novoselov, I. V. Grigorieva et al., Tunable metal-insulator transition in double-layer graphene heterostructures, Nature Phys. **7**, 958 (2011).

[20] L. Britnell, R. M. Ribeiro, A. Eckmann, R. Jalil, B. D. Belle, A. Mishchenko, Y.-J. Kim, R. V. Gorbachev, T. Georgiou, S. V. Morozov, A. N. Grigorenko, A. K. Geim, C. Casiraghi, A. H. Castro Neto, K. S. Novoselov, Strong Light-Matter Interactions in Heterostructures of Atomically Thin Films, Science **340**, 1311 (2013).

[21] L. Britnell, R. V. Gorbachev, R. Jalil, B. D. Belle, F. Schedin, M. I. Katsnelson, L. Eaves, S. V. Morozov, A. S. Mayorov, N. M. R. Peres, A. H. Castro Neto, J. Leist, A. K. Geim, L. A. Ponomarenko, and K. S. Novoselov, Electron Tunneling through Ultrathin Boron Nitride Crystalline Barriers, Nano Lett. **12**, 1707 (2012).

[22] L. Britnell, R. V. Gorbachev, R. Jalil, B. D. Belle, F. Schedin, A. Mishchenko, T. Georgiou, M. I. Katsnelson, L. Eaves, S. V. Morozov, N. M. R. Peres, J. Leist, A. K. Geim, K. S. Novoselov, and L. A. Ponomarenko, Field-effect tunneling transistor based on vertical graphene heterostructures, Science **335**, 947 (2012).

[23] L. Britnell, R. V. Gorbachev, A. K. Geim, L. A. Ponomarenko, A. Mishchenko, M. T. Greenaway, T. M. Fromhold, K. S. Novoselov, and L. Eaves, Resonant tunnelling and negative differential conductance in graphene transistors, Nat. Commun. **4**, 1794 (2013).

[24] A. Mishchenko, J. S. Tu, Y. Cao, R. V. Gorbachev, J. R. Wallbank, M. T. Greenaway, V. E. Morozov, S. V. Morozov, M. J. Zhu, S. L. Wong, F. Withers, C. R. Woods, Y.-J. Kim, K. Watanabe, T. Taniguchi, E. E. Vdovin, O. Makarovsky, T. M. Fromhold, V. I. Fal'ko, A. K. Geim, L. Eaves, and K. S. Novoselov, Twist-controlled resonant tunnelling in graphene/boron nitride/graphene heterostructures, Nat. Nanotechnol. **9**, 808 (2014).

[25] T. Georgiou, R. Jalil, B. D. Belle, L. Britnell, R. V. Gorbachev, S. V. Morozov, Y.-J. Kim, A. Gholinia, S. J. Haigh, O. Makarovsky, L. Eaves, L. A. Ponomarenko, A. K. Geim, K. S. Novoselov, and A. Mishchenko, Vertical field-effect transistor based on graphene-WS_2 heterostructures for flexible and transparent electronics, Nat. Nanotechnol. **8**, 100 (2013).

[26] J. Jung, A. M. DaSilva, A. H. MacDonald, and S. Adam, Origin of band gaps in graphene on hexagonal boron nitride, Nat. Commun. **6**, 6308 (2015).

[27] J. Jung, A. Raoux, Z. Qiao, and A. H. MacDonald, *Ab initio* theory of moiré superlattice bands in layered two-dimensional materials, Phys. Rev. B 89, 205414 (2014).

[28] See Supplementary Material for detailed derivation.

[29] In this work, we ignore the inessential effect of lateral inhomogeneity on tunneling due to finite size of the graphene layers. The lateral dimensions of graphene layers in tunneling experiment typically $\gtrsim \mu$m, which is much larger than the thickness of the spacer $\sim$ nm. A consideration of finite-size effect can be found in Ref. [30] for conventional double quantum well systems.

[30] O. E. Raichev and F. T. Vasko, Electron transport in double quantum wells under the longitudinal size-effect regime, Phys. Rev. B **55**, 2321 (1997).

[31] M. Grifoni and P. Hänggi, Driven quantum tunneling, Phys. Rep. **304**, 229 (1998).

[32] H. Aoki, N. Tsuji, M. Eckstein, M. Kollar, T. Oka, and P. Werner, Nonequilibrium dynamical mean-field theory and its applications, Rev. Mod. Phys. **86**, 779 (2014).

[33] J. Rammer and H. Smith, Quantum field-theoretical methods in transport theory of metals, Rev. Mod. Phys. **58**, 323–359 (1986).

[34] H. Haug and A.-P. Jauho, Quantum Kinetics in Transport and Optics of Semiconductors, 2nd ed. (Springer, Berlin, Germany, 2008).

[35] W.-R. Lee and W.-K. Tse, Dynamical quantum anomalous Hall effect in strong optical fields, Phys. Rev. B **95**, 201411(R) (2017).

[36] W.-R. Lee and K. Park, Dielectric breakdown via emergent nonequilibrium steady states of the electric-field-driven Mott insulator, Phys. Rev. B **89**, 205126 (2014).

[37] N. Tsuji, T. Oka, and H. Aoki, Nonequilibrium Steady State of Photoexcited Correlated Electrons in the Presence of Dissipation, Phys. Rev. Lett. **103**, 047403 (2009).

[38] In our approach, electron thermalization is achieved in two steps: (i) Before switching on the optical field, each graphene layer is tunnel-coupled to a metallic lead on each side to achieve thermal equilibrium resulting in a finite damping rate Γ; (ii) The optical field is adiabatically switched on with a switch-on time that is long compared with other time scales in the system [39, 40]. In this condition, the initial NESS can be adiabatically connected to the thermal equilibrium state [35]. See Ref. [28] for detailed derivation, which includes Refs. [41–50].

[39] V. M. Galitsky, S. P. Goreslavsky, and V. F. Elesin, Electric and magnetic properties of a semiconductor in the field of a strong electromagnetic wave, Sov. Phys. JETP **30**, 117 (1970).

[40] S. Schmitt-Rink, D. S. Chemla, and H. Haug, Nonequilibrium theory of the optical Stark effect and spectral hole burning in semiconductors, Phys. Rev. B **37**, 941 (1988).

[41] Y. Meir and N. S. Wingreen, Landauer Formula for the Current through an Interacting Electron Region, Phys. Rev. Lett. **68**, 2512 (1992).

[42] T. Oka and H. Aoki, All Optical Measurement Proposed for the Photovoltaic Hall Effect, J. Phys.: Conf. Ser. **334**, 012060 (2011).

[43] Y. Zhou and M. W. Wu, Optical response of graphene under intense terahertz fields, Phys. Rev. B **83**, 245436 (2011).

[44] T. Iadecola, C. Chamon, R. Jackiw, and S.-Y. Pi, Generalized energy and time-translation invariance in a driven dissipative system, Phys. Rev. B **88**, 104302 (2013).

[45] H. Dehghani, T. Oka, and A. Mitra, Dissipative Floquet topological systems, Phys. Rev. B **90**, 195429 (2014).

[46] D. E. Liu, Classification of the Floquet statistical distribution for time-periodic open systems, Phys. Rev. B **91**, 144301 (2015).

[47] H. Dehghani, T. Oka, and A. Mitra, Out-of-equilibrium electrons and the Hall conductance of a Floquet topological insulator, Phys. Rev. B **91**, 155422 (2015).

[48] T. Iadecola and C. Chamon, Floquet systems coupled to particle reservoirs, Phys. Rev. B **91**, 184301 (2015).

[49] K. I. Seetharam, C.-E. Bardyn, N. H. Lindner, M. S. Rudner, and G. Refael, Controlled Population of

Floquet-Bloch States via Coupling to Bose and Fermi Baths, Phys. Rev. X **5**, 041050 (2015).
[50] I. Esin, M. S. Rudner, G. Refael, and N. H. Lindner, Steady states and edge state transport in topological Floquet-Bloch systems, Phys. Rev. B **97**, 245401 (2018).
[51] E. K. Irish, Generalized Rotating-Wave Approximation for Arbitrarily Large Coupling, Phys. Rev. Lett. **99**, 173601 (2007).
[52] L. Zheng and A. H. MacDonald, Tunneling conductance between parallel two-dimensional electron systems, Phys. Rev. B **47**, 10619 (1993).
[53] N. Turner, J. T. Nicholls, E. H. Linfield, K. M. Brown, G. A. C. Jones, and D. A. Ritchie, Tunneling between parallel two-dimensional electron gases, Phys. Rev. B **54**, 10614 (1996).
[54] When the layers' chemical potentials are equal, the energy offset between the top and the bottom layers is equal to the interlayer bias voltage. The half-filling condition can be achieved in principle by having top and bottom gate voltages that can be adjusted separately.
[55] For the zeroth-order term, a closed-form analytic expression can be obtained, while the first-order term vanishes under time averaging (see Ref. [28]).
[56] F. T. Vasko, Resonant and nondissipative tunneling in independently contacted graphene structures, Phys. Rev. B **87**, 075424 (2013).
[57] L. Brey, Coherent Tunneling and Negative Differential Conductivity in a Graphene/h-BN/Graphene Heterostructure, Phys. Rev. Appl. **2**, 014003 (2014).
[58] K. A. Guerrero-Becerra, A. Tomadin, and M. Polini, Resonant tunneling and the quasiparticle lifetime in graphene/boron nitride/graphene heterostructures, Phys. Rev. B **93**, 125417 (2016).
[59] We have checked that $\mathcal{E}_c/\Delta = 4$ is sufficient for the tunneling current to achieve convergence within the range of bias voltage $eV/\Delta \leq 4$ (see Ref. [28]).
[60] For strong E, the anti-resonance line shape also deviates from a symmetric inverse Lorentzian profile due to multiphoton excitation processes. Such an asymmetric profile is not captured by the second-order perturbation theory.
[61] S. Kohler, J. Lehmann, and P. Hänggi, Driven quantum transport on the nanoscale, Phys. Rep. **406**, 379 (2005).
[62] J. P. Eisenstein, New transport phenomena in coupled quantum wells, Superlattices Microstruct. **12**, 107 (1992).
[63] If one imagines the formation of Floquet sidebands in two steps: (i) generation of "Floquet copies" via displacement of the undressed conduction and valence bands each by $n\hbar\Omega$ (where $|n| = 0, 1, 2, \dots$); (ii) band-mixing between the Floquet copies, then one can readily understand that the $n < 0$ FVSBs have a higher spectral weight compared to the $n > 0$ FVSBs, because the $n < 0$ Floquet copies of the valence band and $n > 0$ Floquet copies of the conduction band have less overlap and hence less band-mixing that would result in spectral gaps in the quasienergy dispersions.
[64] Here we briefly comment on the case when there is a finite doping in each layer. We expect that the amplitudes of anti-resonance peaks would be modified because each of the forward and backward intraband tunneling contributions will depend on the doping level of each layer. The anti-resonance positions are however unchanged because the resonance condition is preserved.
[65] Using a single laser source to illuminate the system does not preclude the resonant tunneling suppression from occurring. Taking account of wave propagation through the structure, the graphene layer further removed from the laser source will experience a field with a weaker amplitude and a different phase. Even though both layers are driven at the the same frequency, a slight modification is expected in the line shapes and positions of the anti-resonance peaks. However, the periodic structure of anti-resonance sequence is still preserved (see Ref. [28]). Illuminating the system with a long-wavelength laser can therefore minimize the phase difference between the fields at the two layers.